

Wi-Chlorian: Wireless sensing and localization of contact forces on a space continuum

Agrim Gupta, Cédric Girerd, Manideep Dunna, Qiming Zhang, Raghav Subbaraman, Tania Morimoto, Dinesh Bharadia
{agg003,cgirerd,mdunna,qiz127,rsubbaraman,tkmorimoto,dineshb}@eng.ucsd.edu
Univeristy of California, San Diego

Abstract

Contact force is a natural way for humans to interact with the physical world around us. However, most of our interactions with the digital world are largely based on a simple binary sense of touch (contact or no contact). Similarly, when interacting with robots to perform complex tasks, such as surgery, richer force information that includes both magnitude and contact location is important for task performance. To address these challenges, we present the design and fabrication of Wi-Chlorian¹, which is a ‘wireless’ sensor that can be attached to an object or robot, like a sticker. Wi-Chlorian’s sensor transduces force magnitude and location into phase changes of an incident RF signal, which is reflected back to enable measurement of force magnitude and contact location. Wi-Chlorian’s sensor is designed to support wide-band frequencies all the way up to 3 GHz. We evaluate the force sensing wirelessly in different environments, including through phantom tissue, and achieve force accuracy of 0.3 N and contact location accuracy of 0.6 mm.

1 Introduction

Our sense of touch is critical for understanding and interacting with the world around us. Human skin has four types of mechanoreceptors capable of sensing haptic information, including force, vibration, texture, and slip [1], which we rely heavily on when interacting with the physical world. However, due to a lack of force sensing capabilities in a number of emerging technologies, this critical haptic information is often lost. To enable richer interactions with the digital world and/or feedback of task-critical force information during operation of robotic systems, there is a need to improve current force sensing capabilities.

Haptic feedback can lead to more intuitive control of analog variables such as music playback volume, screen brightness, and others. Take an example of wireless ear buds in which the volume can be controlled by pressing with more/less force. This would be far more intuitive than double tapping repeatedly to increase the volume in the current implementations. If these wireless ear

buds had not been space constrained, say like your big screen smartphone, there would have been proxy methods for providing intuitive control besides force control, including swiping gestures on the screen. However, as described, this is not true for other space constrained technologies, such as your smartwatch, where there is insufficient space to swipe to control the brightness of the screen. This is where force sensing really shines and finds tremendous possibilities.

Haptic feedback for robotics poses similar problems, where the sensors must be mounted in difficult locations and must operate within extremely low space constraints. Many robots are remotely teleoperated, typically due to the need to operate in environments that are either hazardous or physically difficult for humans to access. Force sensing in these scenarios is critical, since teleoperation through a remote interface or tool causes the operator to lose their sense of touch, as they are no longer in direct contact with the physical environment. This lack of touch presents a particular challenge in the surgical setting, where robots can offer a number of potential benefits due to increased dexterity and precision compared to manual tools [2]. In addition, the sensing challenge is further exacerbated by the small size of surgical tools, as well as the need for force information not just at the tool tip, but ideally along the length of the tool as well. This exacerbates the need for force sensing from not only requiring the location and magnitude of force, but the sensors should also be easy to attach, easy to read – no wires, low-form factor and batteryless. In fact, force sensing has even been posed as a ‘Grand Challenge’ for further advancement of surgical robotics [3].

Motivated by these requirements, we present Wi-Chlorian, which makes a headway towards this direction with a new force sensor, capable of wirelessly sensing force magnitude and its location. The ability to sense forces wirelessly helps to address some of the difficulties inherent in sensing in remote environments (like in-body). It also helps to overcome issues of scaling when a large number of sensors are needed, since a large number of wires are no longer required. In addition, we have designed Wi-Chlorian as a passive sensor by leveraging backscattering techniques. Rather than having an active RF transceiver with power amplifiers, ADC quantizers, and numerous other electronics, Wi-Chlorian’s force sensors have an antenna, a small identification unit and a force continuum surface, that directly embeds the force

¹Like the popular Midi-Chlorians in Star Wars, Wi-Chlorian makes backscatter sensing sentient to applied force and its location on a space continuum

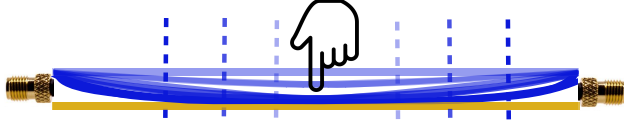


Figure 1: As contact force increases, the top beam bends more and more, and shifts the shorting points (dotted lines) further towards the ends

magnitude and location information in the properties of the signal reflected from the antenna. Such reflection requires minimal power, which can be harvested and therefore simplifies the sensor design.

A natural question arises as to how can contact force, a mechanical entity, and further the location where it is applied, be linked to some RF signal parameters for enabling low-powered wireless force sensing. In this quest to relate these two entities, Wi-Chlorian combines the classical beam bending models and RF transmission line concepts. Whenever a certain force is applied on a surface, a natural effect is to see some sort of deformation/bending occurring near its location of contact (Fig. 1). This bending hinders the propagation of RF signals on this surface, which in turn lead to phase changes in the signal properties. Finally, to realize this conceptual idea, Wi-Chlorian creates a novel sensor surface consisting of two parallel beams with a specialized polymer and a conductive trace on each beam and separated by air. As the force is applied at a specific location, the top beam bends, causing the traces to connect. This phenomena can be viewed as a transmission line shorting which causes a reflection of signals (Fig. 1). As the force increases, the locations of these shorting points further shift to the ends, causing a change in the phase of the reflected signal from both ends. This allows Wi-Chlorian to transduce the force magnitude and location onto the reflected signal phases, to facilitate extremely low-powered force sensing.

From Fig. 1, it becomes apparent that force magnitude and location are related to the phases measured on both the ends of the sensor. To sense phases from both the ends wirelessly, the wireless reader transmits a signal, which is received by the antennas at each end (Fig. 2). The received signal then propagates along the sensor length, accumulating phase changes, until it encounters a shorting point, where the signal is reflected back via the connected antenna. The goal is to measure only the accumulated phase due to signal propagation on the sensor microstrip line, and from both the ends.

To enable sensing of these phases by the wireless reader, the phases from either ends have to be disambiguated and thus each end has to be given an identity. To do so, a naive solution would be to have RF switches toggling with different frequencies on either ends (Fig. 2), with the toggling frequency providing the unique identity

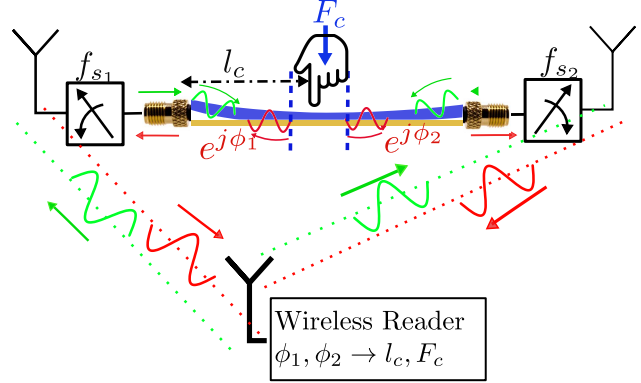


Figure 2: Reflected signal phase changes as the shorting points shifts. Hence sensing phases from the either ends (ϕ_1, ϕ_2) allows force estimation at the wireless reader. For representation purposes, both ends are connected to antennas, however the final sensor design can work with just one antenna

to each of the ends. However, this naive solution do not work, because the two ends are electrically connected to each other via the transmission line, and hence signals will readily leak from one end to the other which would cause intermodulation effects ultimately leading to muddled up identities.

To resolve this issue, Wi-Chlorian comes up with a creative RF switch toggling strategy, which not only provides electrical isolation to combat intermodulations, but at the same time also provides different identities to these ends in terms of different frequency shifts. Hence, the external wireless reader is able to read the phases coming from each of these two ends individually by exploiting this separation in frequency domain, at the same time fooling the sensor into believing that these two ends were never in-fact connected together.

The final piece in Wi-Chlorian is designing the wireless reader, such that it can use any wireless device (like WiFi (OFDM) or LoRa (FMCW)) with wide-band transmission to read the Wi-Chlorian's force and location. The task of the wireless reader is two-fold, first identify the signals coming from the sensor in the myriad of reflections coming from environmental clutter, and then after isolating sensor's signals, track the phase very accurately. Since the wireless phase observed by the reader can also be altered by various entities in the environment, the task of reading phase changes corresponding to sensor only is non-trivial. Hence, Wi-Chlorian designs a novel signal processing algorithm which utilizes periodic wide-band channel estimates to pick up the reflection signatures from the sensor in order to isolate the signal, and then further utilizing this wideband channel estimate to read the phase changes at multiple frequencies, which provide robustness to the phase sensing requirements for the proposed force transduction mechanism.

We designed and fabricated the sensor with ecoflex

soft-polymer material with bending properties which maximizes the phase changes transduced by contact forces, which was retrofitted with a RF-switches and an antenna. The power consumption of our sensor including the switch toggling and clock is under $1\mu\text{W}$ evaluated in TSMC technology node of 65 nm, as flip chip package. The fabricated sensor works for the entire sub-3 GHz verified with the test equipment (vector network analyzer). We evaluated the Wi-Chlorian sensor abilities to report force magnitude and location in multiple different settings in indoors, and inside body like environment using gelatin. We used USRP radios as the readers, and tested the sensor at 900 MHz and 2.4 GHz, which are the two most popular ISM bands. We show that the sensor can be read up to 5 meters of range over the air, and show the algorithm working even when the propagation through over the gelatin based muscle/fat/skin tissue layers composition similar to the human body to demonstrate the surgical applications. We evaluated the performance by using very accurate accuator to provide ground-truth force and contact location. We achieved phase sensing with an accuracy as low as 0.5° , giving us a force resolution of 0.3 N, and location accuracy of 0.3 mm. Finally, we even evaluated our force sensor with a user pressing with his hand, and we achieved force resolution of 0.3 N, and location accuracy of 0.3 mm. In fact, recent HCI work shows that similar resolution ($0.2N$) is required to support force enabled gestures on smartphones and desktop computers [4]. We believe this is the first step towards enabling numerous force sensing applications.

2 Background and Motivation

Haptic feedback and force sensing has been a pertinent problem with robotics and HCI. Although there exist many good haptic feedback solutions to sense point forces, the real challenge in force sensing now lies in sensing forces on a continuum. Sensing forces on a continuum of surface opens up interesting possibilities with robotics, since this sensing modality will finally allow robots to have a sense of touch. The continuum force sensor can thus act like an artificial skin for robots.

A naive way of attempting continuum force sensing would be to have an array of point force sensors spread across the continuum. However, this solution is hardware intensive and would require wiring up all the sensors across the continuum, which hinders the deployment of such sensing solutions [6]. A solution to the wiring problem is usage of ERT (Electrical Resistance Tomography), which associates force readings with voltages induced across an array of sensing electrodes [6–8]. ERT does not require wired connection to each of the electrodes, since it just requires sensing of voltages across the

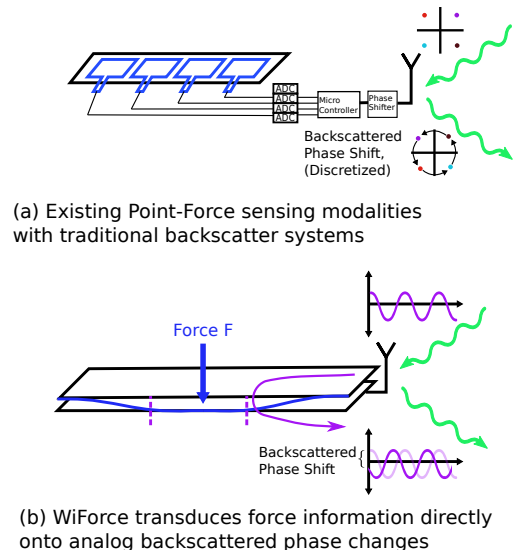


Figure 3: Backscatter design, Wi-Chlorian vs Traditional Backscatter sensor feedback [5]

terminals of the sensor. Hence, it reduces wiring complexity to just interfacing wires towards the ends of the force sensitive area, wherein the voltage across various terminals are sensed and linked to forces and locations.

However, getting a continuum force sensing modality is only one part of the problem. The other part of the problem lies in how these readings are actually fed back. A naive wired feedback approach won't work and will bring us back to square one with the wiring problem. One may argue to connect the sensor via a Bluetooth link, however it would warrant power-hungry components which would require battery connections again getting us back to square one with wiring. A next solution would be to utilize the decades of research in backscatter links [5, 9] and communicate the continuum sensor data over low powered backscattering links. But again here, the solution won't fly since these backscatter links typically work with a RF energy harvester which generates small voltages capable of powering a small RFID chip, and not a big continuum sensing surface having multiple voltages to be sensed via an array of ADCs, and further electronics in a microcontroller required to digitize and buffer the data along.

The key to Wi-Chlorian's design lies in understanding what was inefficient with using a continuum force sensor and a supporting backscatter link. With this strategy, the force sensor gives sensor readings via voltage changes, which are digitized by a ADC, buffered up by a microcontroller. Then using codeword translation [5], or other similar strategies, these information bits are communicated via the backscatter link. Codeword translation works by changing the phase of the incoming signal so that the signals are translated to a different codeword.

The key question Wi-Chlorian answers is, can we do it directly, that is directly transduce force to signal phase, instead of going through the extra electronics in the middle (as visually illustrated in Fig. 3).

Hence, Wi-Chlorian attempts a RF-only approach, where the sensing modality directly transduces force and it's location into wireless signal phase changes, which can be read by a radio over the air. This fulfills both the key requirements for low powered haptic sensing, ability to sense over a continuum of surface and low-powered battery free operation.

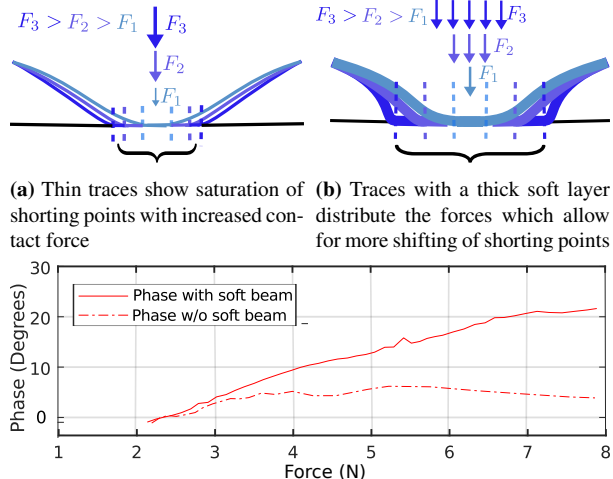
3 Design of Wi-Chlorian

Wi-Chlorian consists of a wireless reader that can read the force magnitude and its contact location from the Wi-Chlorian sensor. Furthermore, Wi-Chlorian's sensor design beyond force magnitude and its contact location, are that it should be robust, low-power, low form-factor, and low complexity, allowing the sensor to be deployed in diverse application scenarios like soft and continuum robots [3]. In this section, we present the design principles of Wi-Chlorian. First, we describe Wi-Chlorian's force sensor, which translates the force applied and its contact location to change in the properties of RF signal (like amplitude, phase). Next, we present novel algorithms to measure change in the RF properties to deduce the force and the contact location wirelessly. Finally, we conclude with a robust channel measurement technique that uses a wireless waveform to read the sensors while rejecting multi-path.

3.1 Force Transduction Mechanism

As a first step to sense force wirelessly, Wi-Chlorian has to form a connection between the contact forces applied in newtons and its contact location to the measurable properties of RF signals like amplitude and phase. The first observation that helps make this connection is that force typically tends to deform/bend physical objects, changing the object's physical dimensions like shape and length. Furthermore, these changes can manifest themselves as changes in the RF signal phase, if the RF signals were propagating through the object. Hence, to design such a wireless force sensor, the strategy would be to choose an object that supports the propagation of RF signals, like transmission lines, and understand how the underlying signal propagation properties would vary due to applying a particular force onto them. These observations lead Wi-Chlorian to its first design principle, wherein it chooses this physical object undergoing shape deformation as a simple microstrip line.

A microstrip line consists of two parallel conducting traces, the signal trace, and the ground trace. A force



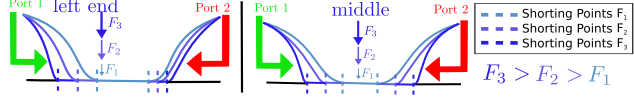
(c) Due to saturation, thin trace sensors do not show much pronounced phase changes as applied force increases

Figure 4: Improving force to phase transduction via aid of soft coflex beam

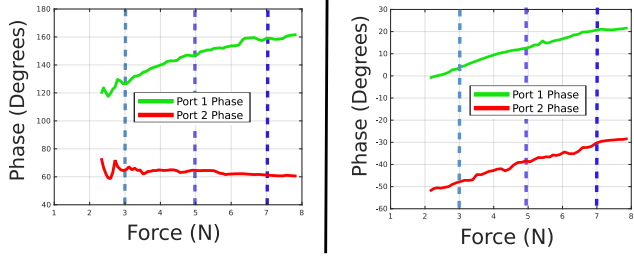
applied to the microstrip line causes the traces to bend and come in contact, which shorts the line and leads to signal reflections. This bending phenomena under the action of a force can be explained by viewing the microstrip line traces as mechanical beams and leveraging popular beam-bending models. The reflections produced by the shorting have different phase properties based on the location of the short. Wi-Chlorian, therefore, combines concepts from RF microstrip lines and beam mechanics to design a sensor that transduces contact forces into measurable RF phase changes.

However, a naive air-substrate microstrip line will not be force-sensitive at all. For such a design, the beam thickness is infinitesimally low, and irrespective of the contact force applied, the traces will touch each other at virtually a single point (Fig. 4a). The contact point invariance leads to a near invariant phase response as force is changed (Fig. 4c), therefore preventing the measurement of force through phase changes.

Wi-Chlorian puts a soft beam on top of the signal trace to make the microstrip lines force sensitive. The soft beam follows predictable mechanical models and distributes the force applied along the length of the trace (For a detailed description on the mechanical models, refer to [10]). The distributed force leads to a finite length of the signal trace to come in contact with the ground trace, creating two distinct shorting points, as shown in Fig. 4b. Further, these shorting points shift towards the ends as the applied force magnitude increases. Varying shifts induce different phase changes since the signals travel lesser distance on the microstrip line before getting reflected at the shorting points. Hence, the reflections caused by higher magnitude forces accumulate lesser



(a) Beam Bending: Shorting points shift further apart as the force magnitude increases



(b) Phase Changes due to Beam Bending: Phase-force profiles for the three scenarios above obtained via VNA experiments

Figure 5: The shifting of shorting points due to increased force changes the reflected phase on both the ports, and depending on the location where force is applied both the ports different phase-force profiles.

phases relative to the reflected phases when lower force was applied. Thus, the soft beam augmented microstrip line allows us to transduce force to phases (Fig. 4c).

However, this beam bending effect manifests itself in the form of a varying phase-force relationship depending on the contact force’s point of application (Fig. 5a). A force applied in the middle of the sensor compresses it symmetrically, and therefore the reflected signals from both the ends show similar phase changes. In contrast, a force that acts asymmetrically will disproportionately compress the smaller length of the beam. Therefore, the end near the smaller length shows a higher phase shift than the end near the longer one. The longer length collapses onto the bottom trace, leading to an almost stationary shorting point as forcing increases (Fig. 5b). This asymmetric behavior of phase change with force contact location necessitates sensing phases from both ends of the sensor. The varying force profile depending on the location of contact also allows Wi-Chlorian to localize the force locations. Thus, the double-ended measurement allows us to estimate the applied force’s magnitude and its location along the sensor length.

3.2 How to Sense Force Wirelessly?

As described in the previous section, knowing phase changes from both ends of the sensor allows for measuring and locating the applied force. This section describes the challenges of measuring these phases wirelessly: First, we delineate the method to get a single-ended wireless phase measurement robust to environmental effects. Then we elaborate on the challenges in extending the measurement to both ends and describe our novel switching design that allows it.

Sensing these phases from either side of the sensor to estimate the force magnitude and location can be done using a wired measurement device like a Vector Network Analyzer (VNA). A VNA typically enables 2-port analysis of a device-under-test (DUT), i.e., it sends RF signals from both ends of the DUT and measures the reflection properties (amplitude and phase). Therefore, the phase changes due to the shorting points can easily be measured in a wired setup using a VNA. However, wirelessly performing the same task is far from trivial. The wireless signal’s phase is easily corrupted by timing offsets, hardware non-idealities, and environmental multipath effects [11]. Further, the concept of obtaining the absolute phase change due is challenging since any wireless phase measurement would also account for the phase accumulated by traveling some distance over the air.

The key idea that allows wireless measurement is the observation that force information is embedded in the differential phase and not the absolute phase. A force applied to the sensor changes the reflected signal’s phase, but the phase changes due to air propagation, environmental effects, and hardware offsets remain fixed. Therefore, the differential measurement allows us to bring out only the difference due to the sensor. The difference manifests as a phase jump due to the creation of shorting points on the sensor. By observing the differential phase from both ends of the sensor, one can infer how much contact force caused this phase jump.

Sensing differential phase from one end of the sensor: To estimate the differential phase from the sensor, an initial requirement is to first decode the signal coming from the sensor. For this, Wi-Chlorian utilizes RF switches toggling at a particular frequency to modulate the reflected signal, similar to RFID based backscatter systems [9, 12, 13]. The tag receives the excitation signal $s(t)$ and reflects $s(t)m(t)$ where $m(t)$ is a square wave, with time period T . Expanding $m(t)$ ’s Fourier series, we get odd harmonics, $m(t) = \sum_{k \in (2i+1), i \in \mathbb{Z}} \frac{1}{|k|} e^{j2\pi k f_s t}$ where $f_s = \frac{1}{T}$. Ignoring the high order harmonics, we get reflected signal as $r(t) = s(t)m(t) \approx s(t)e^{j2\pi f_s t}$. Hence the reflected signal will be shifted by frequency f_s , which allows the reflected signal, $r(t)$, to be isolated from the excitation signal, $s(t)$ in the frequency domain.

Hence, to sense differential phase from the sensor, the wireless reader reads the phases at shifted frequencies, and observes the phase jumps caused by the shifting of contact edges between the traces due to an applied force (Fig. 6). Denote the reflected signal just before/after a contact force was applied as $r_1(t)/r_2(t)$. From, Fig. 6 $\angle r_1(t) = \phi_{\text{full}} + \phi_a$, from the wireless propagation over the air and over the entire length of the sensor. Similarly, $\angle r_2(t) = \phi_{\text{short}} + \phi_a$, since now the signal got reflected back from the shorting point. Thus, the differential phase between $r_1(t), r_2(t)$ would be $\phi_{\text{full}} + \phi_a - \phi_{\text{short}} - \phi_a$, and

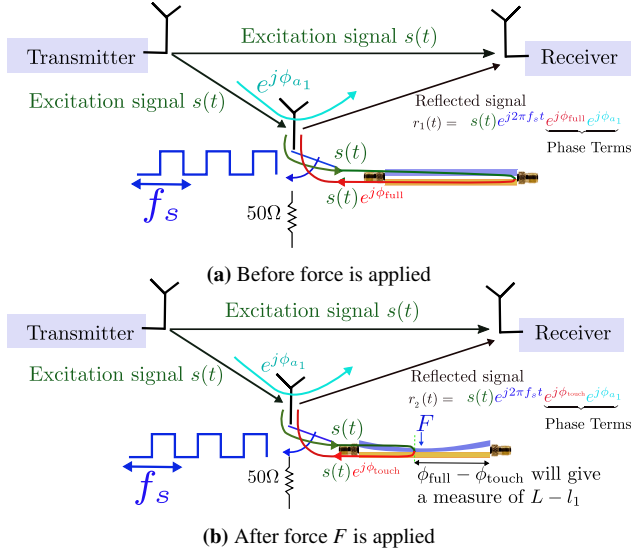


Figure 6: Modulation with a square wave (blue) allows isolating the reflected signal from excitation signal. Observing differential phase ($\angle r_1(t) - \angle r_2(t) = \phi_{full} + \phi_a - \phi_{touch} - \phi_a$) allows to get rid of phase accumulated over the air (cyan) and gives measure of phase change due to shorting of microstrip line

thus the differential phase jump would give us $\phi_{full} - \phi_{short}$. Since ϕ_{full} is the net phase accumulated by the signals by traveling the full length of the microstrip line, this is a fixed quantity that can be calibrated beforehand from accurate VNA readings. Thus, reading the differential phase allows us to estimate $\phi_{full} - \phi_{short}$, and in turn, ϕ_{short} , which is the phase due to the shifting of contact points caused by an applied force.

Sensing differential phase from both the ends of the sensor: A naive extension to the single ended measurement is to have RF switches on both ends of the sensor, toggle them at different frequencies (f_{s1}/f_{s2}), and read the phase jumps at these shifted frequencies. Although this solution to sense phase jumps from both ends is correct in spirit, there is more to the double-ended sensing problem than just simple frequency multiplexing. To estimate the differential phase, it is required to sense the phase before force was applied, in which the sensor acts like a perfectly conducting microstrip line between the two ends. In this scenario, if both the switches are toggled-on, the signals will propagate through the sensor and leak out from the other end. This causes intermodulated reflections, where the reflected signal would be partially modulated by both toggling frequencies. This is visually illustrated in Fig. 7.

The challenge in avoiding the intermodulation effects is that the sensor has to reflect signals from the opposite end when a switch is toggled on. Using reflective RF switches in the off state allows us to make either of the ends reflective, under the restriction that the other

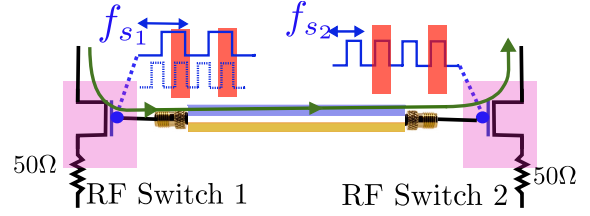


Figure 7: Different freq. clocks introduce intermodulation due to both switches being toggled on (red shaded time instants)

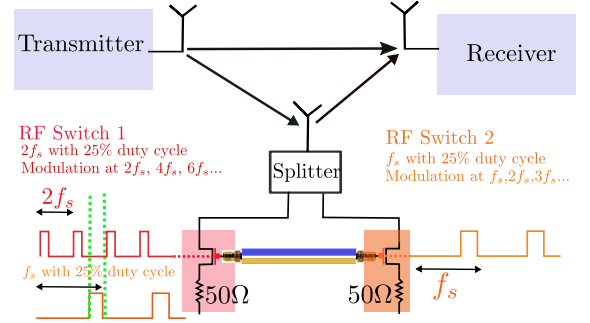


Figure 8: The two-ended sensing approach of Wi-Chlorian. At any time instant, only one switch is toggled on

should be off when one switch is on. The unique insight which allows Wi-Chlorian to have such a on-off scheme is the use of duty cycle properties of square wave Fourier series. In a standard square wave, with 50% duty cycle, all the even harmonics (i.e. every second harmonic) are absent. Similarly, in a wave with 25% duty cycle, every fourth harmonic would be absent. Hence, a frequency f_s , 25% duty cycle square wave will give modulation at $f_s, 2f_s, 3f_s, 4f_s, 5f_s, \dots$. Similarly, a frequency $2f_s$, 25% duty cycle square wave will give modulation at $2f_s, 4f_s, 6f_s, 8f_s, 10f_s, \dots$. Observe that a combination of these 2 clocks will cause interference at $2f_s$, but can be read up individually at f_s for the former clock, and $4f_s$ for the latter clock. Hence, a combination of these 2 clocks can provide separation in the frequency domain. Also, by controlling the initial phases of these two clocks, we can suppress the intermodulation problem as well. This is possible because when one clock is high, the other clock will be guaranteed to be low and vice versa (Fig. 8). Hence, at any given time, only one port will be on, and other port will be reflective open. Further, to reduce the form factor requirements, instead of having 2 antennas, one for each end of the sensor, we can just have just a one antenna design using a splitter. Since the clocking strategy provides separation in the frequency domain, we can add the modulated signals from the either ends via a splitter. Thus, we can read the differential phases at $f_s, 4f_s$ due to new shorting points caused by the bending of the sensor under an applied force F .

3.3 Rejecting Multipath by Reading Forces at Multiple Frequencies

In this section, we describe how Wi-Chlorian uses general wideband signals to measure differential phase across both ends of the sensor. The key insight of Wi-Chlorian here is to use the general wide-band signal to estimate channel periodically and leverage these measurement to detect the frequency shifts coming from the sensor modulations. Further, going one step ahead, we can even harness tremendous averaging gains by reading the same differential phase over the entire wide-band channel estimates. Therefore, Wi-Chlorian's strategy becomes waveform-agnostic, and can be used with any wideband sensing waveform that allows for periodic channel estimates, such as FMCW, UWB and WiFi-OFDM (11g).

Wi-Chlorian's strategy consists of two steps: The first step involves viewing the frequency shift originating from square wave modulation as an 'artificial-Doppler', since Doppler effects also introduce similar frequency shifts. Wi-Chlorian utilizes an FFT-based technique of sensing these frequency shifts, which works very similar to how Doppler is traditionally sensed via wideband sensing waveforms like FMCW and UWB [13]. We show that this algorithm works with a lower bandwidth (12.5 Mhz) OFDM based channel sounding approach. Since force information is in the form of phase changes unaffected by environmental effects and air propagation, we do not need absolute time-of-flight measurements, avoiding very high bandwidth (100s of MHz) typical of FMCW/UWB.

The algorithm to estimate the two-ended differential phase embedded inside the wideband channel estimates is visually illustrated in Fig. 9. Say we are estimating the channel periodically after every T seconds, with frequency steps of F (this could be subcarrier spacing/sweep step in OFDM/FMCW based waveforms). We denote $H(kF, nT) = H[k, n]$ where k is subcarrier index and n is time index. Now, if there are M multipaths in addition to the signal coming from the sensor, we can write the channel estimates as $H[k, n] = \sum_{i=1}^M \alpha_i e^{-j2\pi k F \frac{d_i}{c}} + (s_1(nT)e^{-j\phi_n^1} + s_2(nT)e^{-j\phi_n^2})\alpha_s e^{-j2\pi k F \frac{d_s}{c}}$

Here, α_i is the attenuation factor for the i -th path, d_i is the distance separation between the TX-reflector and reflector-RX, and ϕ_n^1, ϕ_n^2 is the phase accumulated from the RF propagation in the microstrip line sensor at time index n from sensor end 1 and sensor end 2. $s_1(t), s_2(t)$ are the double-ended sensor modulation as per the duty cycled clocking strategy discussed earlier. Expanding them as harmonics, we get $s_1(t) = \sum_{p \neq 4q, q \in \mathbb{Z}} a_p e^{j2\pi p f_{s_1} t}$, $s_2(t) = \sum_{p \neq 4q, q \in \mathbb{Z}} a_p e^{j2\pi p f_{s_2} t}$. We have $f_s = f_{s_1} = 0.5 f_{s_2}$ and thus modulations at $f_s, 4f_s$. Ignoring the higher harmonics and the con-

stant factors a_p associated with the Fourier expansion for brevity, we get $H[k, n] = \sum_{i=1}^M \alpha_i e^{-j2\pi k F \frac{d_i}{c}} + \alpha_s e^{-j2\pi k F \frac{d_s}{c}} (e^{j2\pi f_s n T} e^{-j\phi_n^1} + e^{j2\pi(4f_s)nT} e^{-j\phi_n^2})$

Now, to isolate the signal coming from the sensor, we take FFT over the n -th index, to obtain $\tilde{H}[k, f]$. We observe N channel snapshots and take the following transform:

$$\tilde{H}[k, f] = \sum_{n=1}^N H[k, n] e^{-j2\pi f n T} \quad (1)$$

Observe that for this transform, the nyquist frequency would be $\frac{1}{2T}$, and hence, f_s has to be chosen such that $4f_s \leq \frac{1}{2T}$. Hence, assuming ϕ_n^1, ϕ_n^2 stay constant over the period of N snapshots, at $f_s, 4f_s$, we have,

$$\begin{aligned} \tilde{H}[k, f_s] &= \sum_{n=1}^N H[k, n] e^{-j2\pi f_s n T} = \alpha_s e^{-j2\pi k F \frac{d_s}{c}} e^{j\phi_n^1} \\ \tilde{H}[k, 4f_s] &= \sum_{n=1}^N H[k, n] e^{-j2\pi 4f_s n T} = \alpha_s e^{-j2\pi k F \frac{d_s}{c}} e^{j\phi_n^2} \end{aligned} \quad (2)$$

This draws a parallel to how Doppler is sensed from wideband sensing algorithms, and switching in fact gives the sensor an 'artificial Doppler' which can be sensed as done above. The switching frequency f_s can be related to an equivalent Doppler, $f_s = \frac{f_c v}{c}$, and thus an object in the environment moving at velocity $v = \frac{c f_s}{f_c}$ would create interference with the sensor signal. However, the chosen f_s is large enough so that this equivalent speed is so high that it wouldn't appear in the environment for the use cases considered. Hence, taking this FFT isolates the signal coming from the sensor and nulls out the multipath clutter in the environment.

Recall that while writing Eqn. (2), we assumed ϕ_n^1, ϕ_n^2 stay constant over the period of N snapshots. Basically, this assumes that the force acting on the sensor stays almost constant for about N snapshots, which is a reasonable assumption given it requires some time for mechanical beams to relax and get to steady state under the action of force. Said differently, wireless sensing occurs at much higher sampling rate (about order of MHz), whereas the mechanical forces are much slower (take about 0.5-1 seconds to stabilize).

Thus, Wi-Chlorian designs an algorithm to sense these phase differences from the filtered harmonics, and ultimately map them to applied force. The algorithm divides the channel estimates into groups of N , referred to as 'phase-groups'. For each phase-group we first take the harmonics FFT as described earlier and obtain $2K \times 1$ vector from Eqn.2 for FFT frequency $f_s, 4f_s$. Assuming there are N_g such phase groups, and for all N samples of g -th group, $\phi_n^1, \phi_n^2 \approx \phi_g^1, \phi_g^2 \forall n \in \{1, 2, \dots, N\}$. The output at g -th phase group, k -th subcarrier, after harmonics

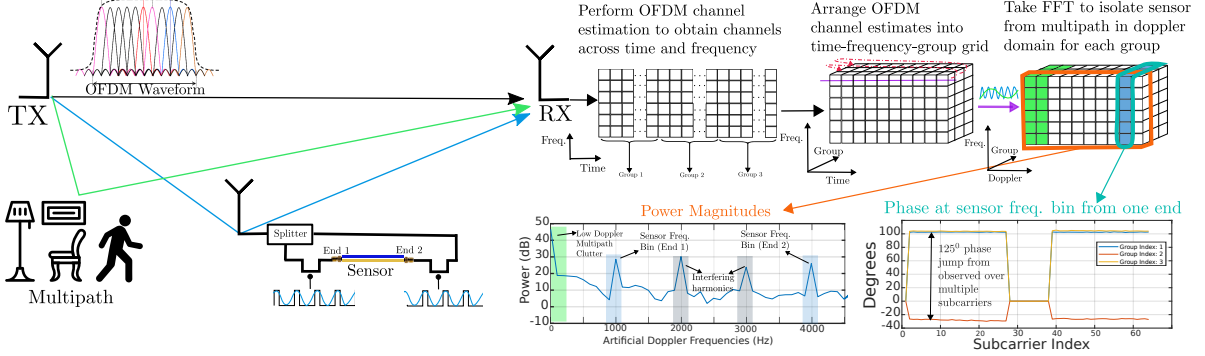


Figure 9: Wi-Chlorian’s sensing algorithm which utilizes wideband channel estimates to isolate the signal from multipath in Doppler domain. Finally, by grouping the channel estimates into ‘phasegroups’, Wi-Chlorian can read phase changes over multiple subcarriers which allows for averaging gains to make the phase sensing robust and accurate
 FFT at $f_s, 4f_s$, is denoted as $P_1[k, g], P_2[k, g]$, and has the following form:

$$\begin{aligned}
 P_1[k, g] &= \tilde{H}[k, f_s] = \alpha_s e^{-j2\pi k F \frac{d_s}{c}} e^{j\phi_g^1} \\
 P_2[k, g] &= \tilde{H}[k, 4f_s] = \alpha_s e^{-j2\pi k F \frac{d_s}{c}} e^{j\phi_g^2}
 \end{aligned} \quad (3)$$

Hence, we can obtain the phase change between 2 groups $\phi_{g+1}^1 - \phi_g^1, \phi_{g+1}^2 - \phi_g^2$ due to some contact force applied during this time by taking conjugate multiplication:

$$\begin{aligned}
 \tilde{P}_1[k, g] &= P_1[k, g+1] * \text{conj}(P_1[k, g]) \\
 &= \alpha_s e^{-j2\pi k F \frac{d_s}{c}} e^{j\phi_{g+1}^1} \alpha_s^* e^{j2\pi k F \frac{d_s}{c}} e^{-j\phi_g^1} \\
 &= |\alpha_s|^2 e^{j(\phi_{g+1}^1 - \phi_g^1)}
 \end{aligned} \quad (4)$$

Hence, we have

$$\angle \tilde{P}_1[k, g] = \phi_{g+1}^1 - \phi_g^1, \angle \tilde{P}_2[k, g] = \phi_{g+1}^2 - \phi_g^2 \quad (5)$$

for each subcarrier k . We can assume that the required phase change is almost constant with subcarrier index given the low bandwidth, ($f_c + k\Delta F \sim f_c$). This allows us to measure the phase change at multiple subcarriers and finally we can take an average (over subcarrier indices k) here to get to one sample value of phase change from either sides of the sensor. Thus by observing $\text{mean}(\angle \tilde{P}_1[k, g]), \text{mean}(\angle \tilde{P}_2[k, g])$ over multiple phase groups, we can identify the action of a contact force F which acts on the sensor and induces these phase changes.

4 Sensor Design and Implementation

4.1 Sensor RF Interfacing

To support the two broad applications targeted by Wi-Chlorian, the sensor must give good RF propagation performances at 900 MHz (for in-body sensing applications) and at 2.4 GHz (to be compatible with Wi-Fi/Bluetooth

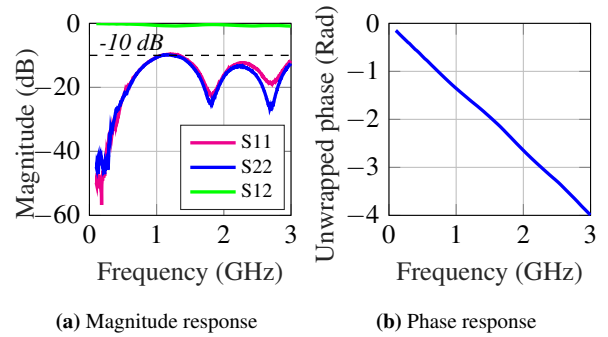


Figure 10: RF propagation characteristics in the sensor. Across the entire 3 GHz frequencies, S11 is below -10 dB, S12 is about 0 dB with linear phase.

standards). From our simulations (Section 9), we expect that by having the ratio between trace width and sensor height to be around 4 : 1, we should get good impedance matching. Hence, we design an air substrate microstrip line with trace width of 2.5 mm, ground trace width of 6 mm and height of 0.63 mm, for a sensor length of 80 mm. To verify the impedance matching, we assess the RF design performance of the sensor in terms of insertion/thru losses. For this, we perform a 2 port amplitude/phase analysis using VNA. As visible in Fig. 10, this leads to a S11/S22 ratio below -10 dB over the entire frequency range from 0 to 3 GHz, along with linear S12 phase, which justifies the broadband nature of the sensor.

4.2 Forming the Sensor Model

After having verified the RF properties of the sensor, we form a sensor model that allows to obtain force magnitude and force location from the phases observed at both ends of the sensor. To achieve this, we exert forces on the sensor at 5 locations, namely 20, 30, 40, 50 and 60 mm. We expect the beam to show a symmetric phase changes on both the ends when tested at the center point, and asymmetric phase changes for the end

points. This happens since the beam bends in a different manner as described in Section 3.1. When pressed on the end points, the port near the pressing location would show more phase change, whereas the other end essentially shows a constant phase as force increases. For this testing, we use the setup visible Fig. 11, where an indenter allows to apply a force at a given location on the sensor, and a load cell on which the sensor is attached allows to collect the values of force magnitudes applied. As seen clearly in the 20/40/60 mm figures in Table 1, the phases do follow the beam bending model as discussed above, since 40 mm testing shows symmetric behaviour, whereas for 20/40 mm, one of the ends show a constant phase as force magnitude is increased.

We now use the data obtained by applying force at all 5 locations, and compute a cubic-fit to make a model that allows to compute the force magnitude and force location based on the measured phase changes. To confirm the validity of the model, we assess it at an intermediate point (55 mm), and plot the phase-force profile as predicted by the model alongside the ground-truth profile we collect from the VNA. As visible in Table 1, all graphs for a force application at 55 mm overlay on each other, which confirms the reliability of the computed model.

4.3 Clock Design and RF Switches

To encode the phase changes caused by different shorting positions on the microstrip line due to application of a force, we utilize 2 RF-switches with the duty cycled clocking strategy described in Section 3.2. Recall that to sense forces, Wi-Chlorian measures phases when the sensor is not under a contact force, and when the sensor is touched with a contact force F , and conjugates these phases to remove extra phase due to air. Hence, for our prototype, we require the use of ‘reflective RF-switches’ since we rely on differential phases between no-contact and contact. If we instead use an absorptive switch, the

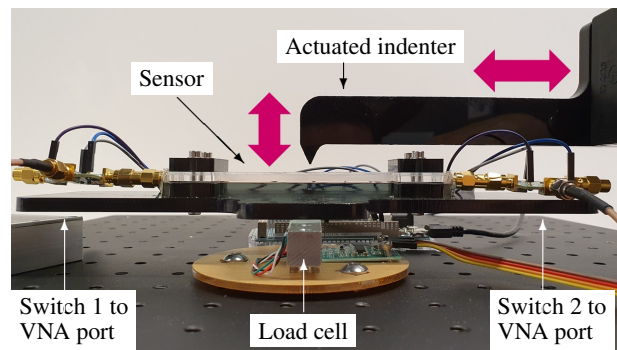


Figure 11: Experimental setup for the application of forces at known locations with an actuated indenter, and measure of the force applied with a load cell for the ground truth.

phase when the sensor is not under a contact force would be unreliable as the signals would get absorbed instead of being reflected back. We use the HMC544AE from Analog Devices in our prototype.

The final component in our prototype design is the clock source. We use the timer channels in Arduino Due [14] with an Atmel SAM3X8E ARM Cortex-M3 processor to generate the duty cycled clock source as described in Section 2. We generate a 25% duty cycled 1000 kHz square wave, and a 75% duty cycled 2000 kHz square wave to modulate the two RF switches. This gives us interference-free modulation at 1000, 4000 kHz.

Hence our sensor prototype consists of five components, shown in Fig. 15, the microstrip line sensor, 2 RF switches, a clock source, a splitter to combine outputs of the 2 switches and one antenna to communicate the backscattered phases to the wireless reader. Furthermore, the entire design with clock, switch was simulated in TSMC 65 nm technology and reported power consumption under less than $1\mu\text{W}$.

4.4 Wireless Reader Implementation

The main task of the wireless reader is to transmit the OFDM waveform and periodically estimate the channel, so that phase changes at the shifted frequencies from the sensor can be read wirelessly. To perform the channel estimation, we utilize a 64 subcarrier, 12.5 MHz OFDM waveform, with a sub-carrier spacing of 195 kHz. We test this for both center frequency of 900 MHz and 2.4 GHz. We use separate antennas for transmission and reception, and use the same USRP N210 SDR [15] for both functions. Since the transmit and receive chains are on the same device, they are synchronized and will not show frequency/phase offsets. We emphasize here that the arduino clock is not synchronized with the other elements of the system since the force sensor is deployed as a separate entity.

We use a 320 sample long OFDM preamble padded with 400 zeros for the channel estimate. At the sampling rate used, this translates to fresh channel estimates every $T = \frac{720}{12.5 \times 10^6} = 60 \mu\text{s}$. Recall that to sense harmonics, the maximum harmonic frequency which can be sensed would be $|f_{\text{max}}| = \frac{1}{2T} \approx 8.7 \text{ kHz}$ due to the Nyquist Limit. We therefore chose our sensor clock frequencies to be 1,2 kHz, which would give modulation at 1,4 kHz, and falls comfortably within measurable limits.

5 Experimental Evaluation

Armed with a sensor model to get from phases to force magnitude/location, as well as wireless reader and sensor implementation to enable backscatter sensing capabilities, we now evaluate the wireless performance of our

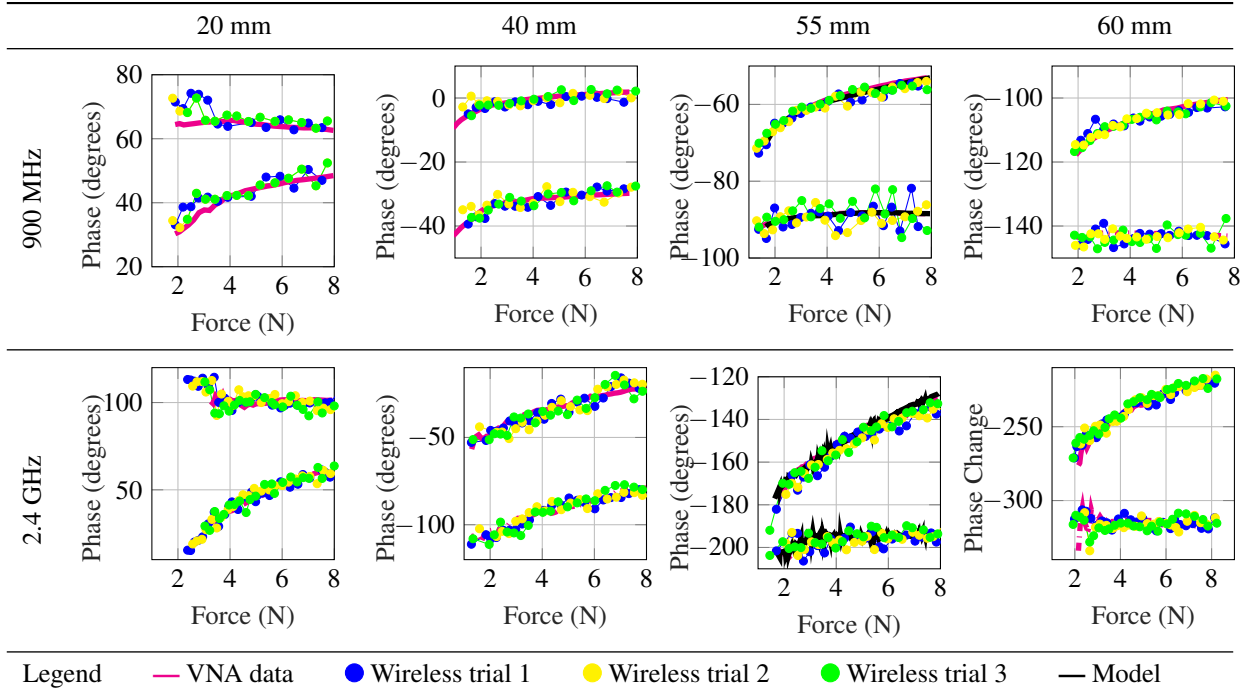


Table 1: Phase measured with the VNA overlapped with the model, and phase measured wirelessly with the presented algorithm.

sensor in different indoor environments. The developed sensor model is first used to estimate the force magnitude and location exerted on the sensor, and this predicted force magnitude/location is compared to ground truth readings from the load cell and actuator position, as shown in Fig. 12. In addition, we plot empirical CDFs, which allow us to understand the accuracy of our sensing solution. We also show that the sensing methodology developed even works under when the wireless propagation occurs through tissue phantoms made to emulate human tissues. Finally, we show that the force sensing works not only with the precision touches of the actuator, but can also detect the force and contact location when a hu-

man interacts with the sensor via finger touches.

5.1 Wireless Performance Evaluation

The first step in the wireless performance evaluation is to verify if the force magnitudes and locations estimated using the model agree with the ground truth collected from the load cell and the indenter position. For this purpose, the setup illustrated in Fig. 12 is used. Forces between 0 and 8 N are applied to the sensor at 20, 40, 55 and 60 mm, similarly to the VNA experiment detailed in Section 4.2. From Table 1, we can clearly see that wireless sensing is able to follow the curves from the VNA, as well as the model predicted curve at 55 mm very closely. Hence, this allows to validate the wireless sensor implementation.

Using the estimated values of force magnitudes and force location to the ground truth, i.e. indenter location and load cell readings, we plot empirical CDFs to evaluate the wireless performance metrics. In Fig. 13, we see that median error of force magnitude estimation of Wi-Chlorian is 0.56 N when being read at 900 MHz, and 0.34 N when being read at 2.4 GHz. These results are satisfactory, since the errors are a fraction of the operating range of the sensor, which is approximately 8 N. One can observe that the error is lower at high frequency. Indeed, since the wavelength is lower, higher frequency signals accumulate more phases for the same travelled distance, compared to lower frequency signals. Another observation from Fig. 13 is that the sensor works uniformly across its length, i.e. error CDFs are similar when plot-

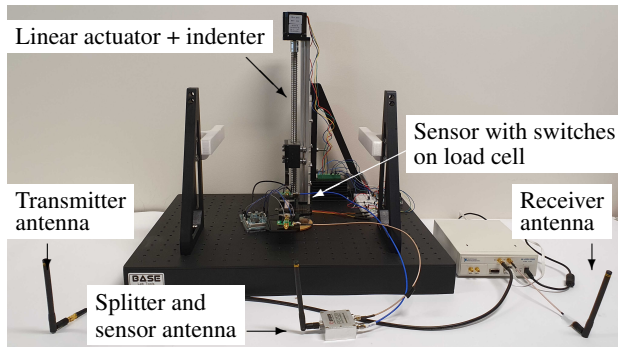
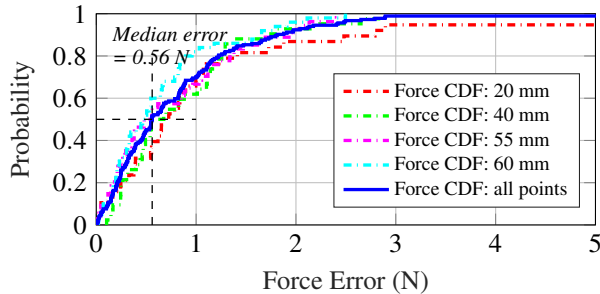
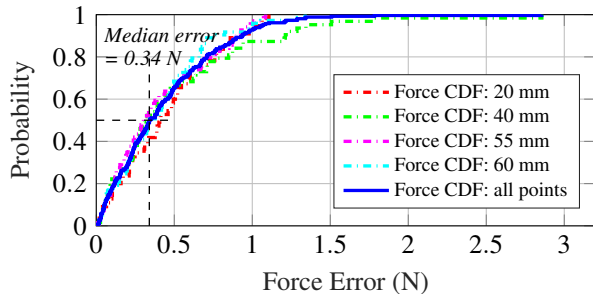


Figure 12: Experimental setup for the assessment of the wireless performance of the sensor. The distance between TX and RX antenna is roughly 1 m and the sensor antenna is placed equidistant at 50 cm away from either of them



(a) Force CDF, center frequency 900 MHz.



(b) Force CDF, center frequency 2.4 GHz.

Figure 13: Force CDF Plots. For testing at individual points, the error is comparable to the combined CDF for which readings across the length are collected. Hence, the performance of our sensing strategy remains good throughout the length of the sensor.

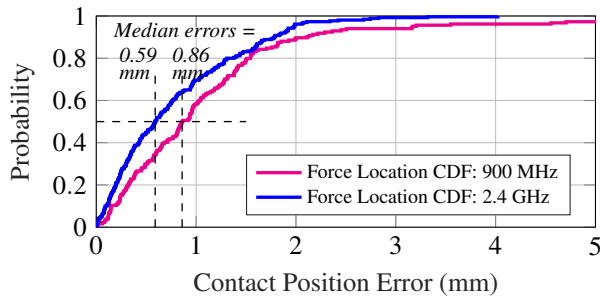


Figure 14: Force Location CDF Plots.

ted for touching at individual locations with increasing magnitude of forces.

Proceeding similarly, the median errors on the estimated force location is 0.86 mm at 900 MHz, and 0.59 mm at 2.4 GHz, as visible in Fig. 14. Similar to force magnitude CDFs, performance is better at a higher frequency, since more phase change is accumulated per unit length at higher frequencies, enabling finer location estimation. These location results are satisfactory, with about 5 times higher accuracy than reported in recent work [16, 17], where errors are in the order of magnitude of centimeters.

5.2 Testing with Tissue Phantoms

We now assess the performance of our sensor through human tissue, which necessitates a frequency of 900 MHz over 2.4GHz, which is attenuated in such environment [18, 19]. Wireless signals undergo huge losses when they propagate through human tissue, since these tissues are typically materials with high dielectric constants (with $\epsilon_r > 10$) [20]. Further, the propagation is hampered via refraction and total internal propagation effects, which exacerbate the losses. For this purpose, we use the setup visible in Fig. 15. It consists in a tissue phantom composed of three layers (muscle, fat and skin, and thickness of 25, 10 and 2 mm, respectively), with dielectric properties selected to mimic human tissue properties, as in [21].

During these experiments, we observe that there was around 110 dB two-way backscatter loss from the TX-sensor and sensor-RX, for center frequency 900 MHz, when communicating through the tissue phantom. However, the direct path TX to RX signal had about 10-15 dB loss. The dynamic range of the USRP SDR we use was around 60 dB, because of which we can't decode the weak backscattered signal under the presence of the much stronger direct path signal. Hence, for these experiments, we isolated the TX and RX with a metal plate for this experiment. Because of the metal plate, the direct path loss increased to about 60 dB, which allowed us to decode the 50 dB lower backscattered signal at the receiver using the 60 dB dynamic range ADC of the USRP. For this experiment, we apply contact force at 60 mm on the sensor. We obtain similar performance as with the over-the-air tests, with the median force error increasing slightly from 0.56 N to 0.62 N (Fig. 16). These results demonstrate the robustness of Wi-Chlorian's wireless capabilities, since the sensing algorithm was able to decode force readings from a weaker signal through the tissue phantom. In future works, the metal blockage can be replaced by more sophisticated self-interference canceling strategies, however, this is beyond the scope of the current paper.

5.3 Getting More Than Finger Touch: Measuring Fingertip Forces

We now motivate a UI use case, which has the potential to improve and change the way users interact with digital devices. For this purpose, we select a center frequency of 2.4 GHz for our sensor, which is well-adapted to Wi-Fi and Bluetooth devices.

To assess the relevance of our sensor for such applications, we press the sensor with fingertip, with varying force levels to convey different commands. We conduct a user study where an operator has to press the sensor

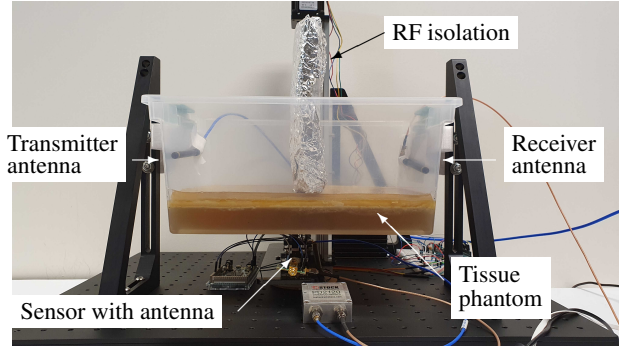
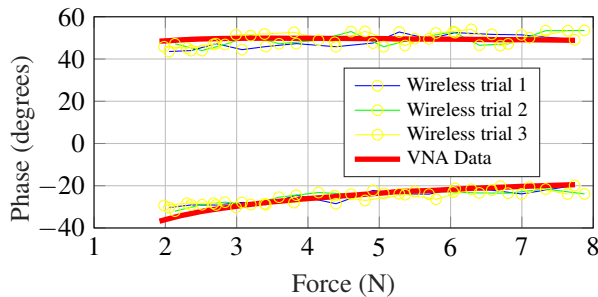
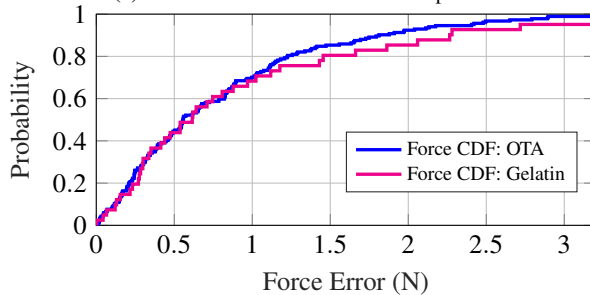


Figure 15: Experimental setup for the assessment of the wireless performance of the sensor through human tissue.



(a) Wireless Phase vs Load cell force profile.

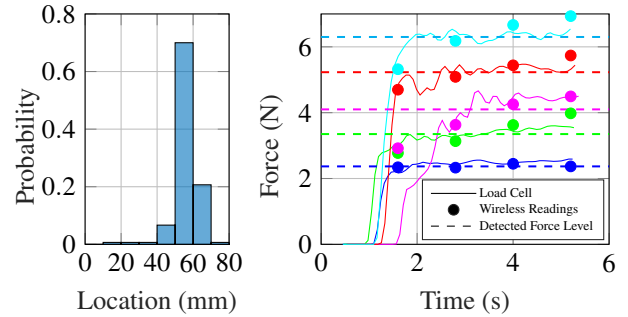


(b) Force Magnitude CDF.

Figure 16: Wireless Sensing results for pressing at 60mm under the tissue phantom setup.

at the location 60 mm. We plot the force readings from the load cell in real time, and use this real-time plot to give the users visual cue to settle in to some force level. Then, we estimate these force levels using Wi-Chlorian to evaluate if it can support these sensing capabilities.

Fig. 17 shows the evaluation results of Wi-Chlorian’s experiments. From Fig. 17a one can see that the sensor could accurately detect the pressing location, which was 60 mm, with sufficient accuracy, considering the fact that a typical human fingertip has a width and thickness of approximately 10 mm. Further, in Fig. 17b, we see how Wi-Chlorian is able to get more than just binary touch sensing results shown in prior work. Not only can Wi-Chlorian detect the point where a finger touched the sensor, going one step ahead, Wi-Chlorian is able to detect



(a) Histogram for contact force location.

(b) Force Magnitude CDF.

Figure 17: Wireless Sensing results for pressing at 60 mm with increasing force levels via a fingertip. From the histogram plot one can see that all the touch interactions at 60 mm touching point were classified to be at the correct location. From the force versus time plot, it is clearly evident that Wi-Chlorian was able to estimate the increasing force levels accurately

the force profiles of the touch interactions as well, which motivates much improved UI use cases by getting more than just touch/no touch information.

5.4 Wi-Chlorian’s performance with distance

Finally, we evaluate our sensor and wireless reader design over a range of distances. For this experiment, we place the TX antenna, sensor antenna and RX antenna along a straight line. The TX antenna is placed 4 m away from the RX antenna, and the sensor is moved from the mid-point, which is 2 m away from both to distances, closer to the RX antenna, and farther away from the TX antenna. The TX power is set to 10 dBm, and the center frequency for this experiment was 900 MHz. We can observe that the sensor gives accurate and satisfying phase stability of less than 1° even at a distance of 1 m, 3 m from the RX/TX, and acceptable within 5° performance even at the worst 2 m, 2 m distance from the TX/RX. These operating distances are comparable with previously shown evaluations with RFID based backscatter at 900 MHz [16], which tested sensing at a maximum distance of 2 m from the RFID reader.

6 Discussions and Applications

The most natural usecase for such wireless haptic feedback lies in surgical robots and tools. Human hands are extremely dexterous, and provide unparalleled sensory feedback which enable very precise operations required for a surgery. However, we need tools and robots to emulate the human hands when it is not possible to use hands for the surgery, due to narrow openings and

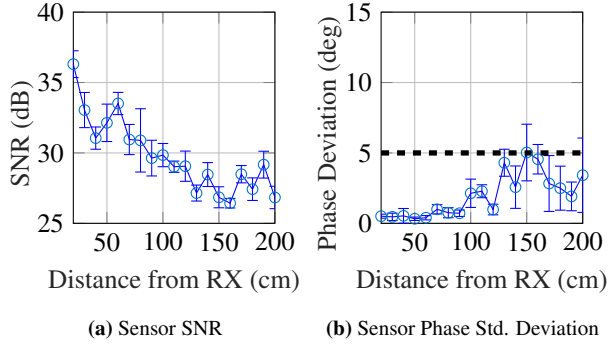


Figure 18: Testing Wi-Chlorian over a range of distances

potentially risky subcutaneous operations. Thus, ideally like hands, surgeons should get haptic feedback from the tools/robots they are operating, which involves feedback of both contact force magnitude and contact location. However, such haptic feedback is generally not available in practice, and the main reasons have been that force sensing modalities are still not evolved enough to support these applications [22–26]. Loss of haptic feedback increases the training time for surgeons, increases risk of surgical errors and hinder the closed-loop operation for robot assisted surgeries [27–30].

One of the main reasons which hinder the deployment of force sensors for this usecase is the wiring requirement of such sensors, which consists of both the physical area costs of wiring an array of sensors around the tool/robot [6, 31], and the electrical risks of potential current arcing from these wires [32]. Wi-Chlorian tries to bridge this gap by creating a 1-D continuum sensor, instead of a wired sensor array, which can sense and localize the contact force acting, with lowest power requirement possible. In fact, the power requirements are so frugal that it can achieve the elusive goal of battery-free haptic feedback, by meeting the power requirements via energy harvesting solutions.

Although the current form factor and sensor interfacing hinders direct usecase of Wi-Chlorian’s sensor in more complex surgical tasks requiring force feedback like cardiac ablation [29], preretinal membrane peeling [33]. However, the sensor can solve a major problem in laparoscopy, which is the fulcrum effect due to lack of haptic feedback [34]. Fulcrum effect is caused due to lever effect caused by contact forces between the body and surgical tool, at the entry point of the surgical incision. Due to lack of feedback on both the magnitude of force and location, the tool tend to slip, which causes risks of tissue damage. A laparoscopic surgical tool augmented with a Wi-Chlorian sensor to determine and localize the contact force can prevent this fulcrum effect since the surgeon can do a closed loop correction based on this haptic feedback.

Apart from surgical applications, sensing contact force and location can be extremely useful for robotic tasks which require a manipulator/gripper. Robotic manipulators need this haptic feedback to determine how firmly and how properly have they grasped a particular object [35, 36]. People have attempted doing this via vision induced haptics [37, 38], however, these typically require computationally intensive algorithms, and fail to meet the required temporal rate of feedback required to determine if the grasp of the object is loosening and slipping [39]. However, since wireless sensing is not bound to such issues, and can be made near real-time. Thus, such sensors can be used for direct and low-latency haptic feedback to improve robotic manipulation operations.

Alongside the robotics centered applications, force sensing can have many latent and currently incomprehensible applications in next generation HCI, AR-VR interfaces. Smart surfaces and smart homes have been an active area of research, with touch sensing touted to a game changer for ubiquitous computing [40–42]. Force sensing will add more depth to these touch sensing solutions, and can lead to some unforeseen applications.

7 Future Work

Extending to 2-D continuum: The current sensor prototype of Wi-Chlorian consists of sensing and localization on a 1-D continuum. To extend this sensing to a 2-D continuum, we can deploy multiple Wi-Chlorian sensors placed next to each other. These sensors will be toggling at different frequencies, and hence will show up in separate doppler bins in the wideband sensing algorithm (Section 3.3). Hence, by reading phase changes from multiple Wi-Chlorian sensors, we can infer the location and contact force magnitude on the 2-D continuum spanned by these multiple sensors. Some hindering factors to this 2-D extension are interpolation of sensor readings when contact is actually in the no man’s land between the 2 sensors, and addressing multiple touch points simultaneously, which will be explored in future works.

Reducing the form factor: Wi-Chlorian is the first work which presents such a low-powered sensor, and thus naturally leads the way to realize a battery-free haptic feedback. The current sensor prototype of Wi-Chlorian is 80 mm long, and about 10 mm in height and thickness. With the current form factor, the sensor is not directly applicable for some of the medical applications which need smaller sensors. The sensors can get to the correct form-factor requirements by designing integrated circuits, antenna and the sensor fabrication. To support this reduced mechanical dimensions, from a RF perspective, Wi-Chlorian can read at even higher frequencies, which effectively reduces the electrical length of the sensor as well. Note that we have already demonstrated that it is

possible to design such sensors over a very wide bandwidth (3 GHz). Further reducing the form-factor of the sensor would allow us to sense forces of lower magnitude, which can motivate some of the more finer-touch usecases of haptic feedback, like cardiac/laparoscopic surgeries and others [3]. To make the sensor prototype more flexible, we will explore new fabrication strategies like flexible PCB printing and creating custom RF connectors to get a flexible haptic feedback sensor.

8 Related Work

Force sensors have been developed using a variety of transduction mechanisms, such as capacitive, piezoresistive, piezoelectric, optical, magnetic, and inductive [43]. There are a number of tradeoffs among the various mechanisms, including, for example, sensitivity, spatial resolution, dynamic range, accuracy, reliability, repeatability, power consumption, and size. To meet the requirements of many emerging systems, particularly those where it may be difficult to have a physical wired connection to the sensors, many researchers have been investigating the creation of wireless sensors.

Wireless force sensors: A number of wireless capacitive force sensors that leverage a change in capacitance due to deformation have been recently developed. For example, a flexible capacitive sensor was created for wirelessly measuring strain in tires [44], and a capacitive textile sensor was developed for wireless respiratory monitoring [45]. While the capacitive sensing paradigm can work well for a number of force sensing applications, it is not naturally compatible with wireless sensing. In order to wirelessly transmit force information obtained through capacitive sensing, additional hardware and circuits are needed, complicating the design.

Inductor-capacitor (LC) wireless sensors are passive devices that can remotely sense a number of parameters, including pressure. The working principle of these sensors is based on changes in the capacitance and inductance causing a shift in the resonant frequency, which can be wirelessly measured [46,47]. A number of these LC wireless sensors have been developed for applications including the monitoring of pressures during arterial blood flow [48] and the measure of finger tip forces during athletic activities [49]. However, the resonance frequency of these sensors, in the range of a few hundred kHz to a few MHz [47], cannot be measured by off-the-shelf Wi-Fi or Bluetooth devices, that only work at specific frequencies, far away from the ones considered. This makes these sensors inadequate for consumer-grade electronic devices for instance. These sensors also suffer from short interrogation distances in the range of a few centimeters [47,50].

Alongside the quest to sense the contact forces, there

has been a large body of research on strain sensors [51–55]. In strain sensing, instead of sensing the normal transversal force acting on the sensor, the longitudinal force is sensed. This sensing modality typically tries to sense the change in the length of the sensor, since longitudinal force has a tendency to stretch and elongate the object it is acting upon. Hence, most of the wireless strain sensor exploit the shifts in resonant frequencies to sense strain. Thus, to infer the strain, a wireless reader evaluates the signal strength at multiple frequencies, figures out where a notch is forming in the frequency response, and uses this information to figure out the fundamental frequency, hence the elongation, and finally the acting strain causing this elongation. It is well known that signal strength is a fickle quantity easily corrupted by multipath. Indeed, most of these works show evaluations in a controlled, anechoic environment, and the technology has not been found to be robust to static multipath [52].

Backscatter sensing systems: Recent advancements in ‘backscatter sensing’ has enabled the creation of passive touch interfaces, and researchers have developed systems to sense battery-free touch interaction. Touch sensing has been a well explored use case of RFID-based interactions [16, 17, 56–61]. IDSense [61] utilized the fact that reflected RSS and phase change in a unique way when the RFID chip is touched, and following up on this PaperId [60] even gave a simple manufacturing method by which one could simply use an inkjet printer to manufacture these RFID tags and augment everyday objects with touch interactions. RIO [16] further explored the touch to reflected signal phase mapping to extend touch sensing to multiple RFID tags by utilizing mutual coupling effects, and extended the design further to use custom designed, application specific RFID tags. Livetag [17] presented a similar touch sensing system showing how to sense these touch interactions using Wi-Fi based readers, which can be augmented on the existing Wi-Fi modems, instead of relying on expensive, dedicated readers used by the earlier works.

However, none of these systems could sense force magnitude and were limited to sensing just the position where the tag was being touched in order to sense simple gestures/sliding movements etc. Wi-Chlorian goes one step further and shows how to sense not just the point where you touched, but also the magnitude of that force. Furthermore, we show how to do this with a Wi-Fi based waveform which can co-exist with the current Wi-Fi modems catering to data communication needs and further augment them with the novel sensing paradigm. Also, in comparison with Livetag [17] which required MIMO Wi-Fi APs and certain beamforming modes not catered by most of the modems, Wi-Chlorian can work with COTS Wi-Fi APs with just one antenna.

References

- [1] Victoria E Abreira and David D Ginty. The sensory neurons of touch. *Neuron*, 79(4):618–639, 2013.
- [2] Paula Gomes. Surgical robotics: Reviewing the past, analysing the present, imagining the future. *Robotics and Computer-Integrated Manufacturing*, 27(2):261–266, 2011.
- [3] Jessica Burgner-Kahrs, D Caleb Rucker, and Howie Choset. Continuum robots for medical applications: A survey. *IEEE Transactions on Robotics*, 31(6):1261–1280, 2015.
- [4] Axel Antoine, Sylvain Malacria, and Géry Casiez. Forceedge: controlling autoscroll on both desktop and mobile computers using the force. In *Proceedings of the 2017 CHI Conference on Human Factors in Computing Systems*, pages 3281–3292, 2017.
- [5] Pengyu Zhang, Dinesh Bharadia, Kiran Joshi, and Sachin Katti. Hitchhike: Practical backscatter using commodity wifi. In *Proceedings of the 14th ACM Conference on Embedded Network Sensor Systems CD-ROM, SenSys '16*, page 259–271, New York, NY, USA, 2016. Association for Computing Machinery.
- [6] Hyosang Lee, Kyungseo Park, Jung Kim, and Katherine J Kuchenbecker. Internal array electrodes improve the spatial resolution of soft tactile sensors based on electrical resistance tomography. In *2019 International Conference on Robotics and Automation (ICRA)*, pages 5411–5417. IEEE, 2019.
- [7] Kyungseo Park, Hyunkyung Park, Hyosang Lee, Sungbin Park, and Jung Kim. An ert-based robotic skin with sparsely distributed electrodes: Structure, fabrication, and dnn-based signal processing. In *2020 IEEE International Conference on Robotics and Automation (ICRA)*, pages 1617–1624. IEEE, 2020.
- [8] Hyosang Lee, Hyunkyung Park, Gokhan Serhat, Huanbo Sun, and Katherine J Kuchenbecker. Calibrating a soft ert-based tactile sensor with a multi-physics model and sim-to-real transfer learning. In *2020 IEEE International Conference on Robotics and Automation (ICRA)*, pages 1632–1638. IEEE, 2020.
- [9] Pengyu Zhang, Colleen Josephson, Dinesh Bharadia, and Sachin Katti. Freerider: Backscatter communication using commodity radios. In *Proceedings of the 13th International Conference on Emerging Networking EXperiments and Technologies, CoNEXT '17*, page 389–401, New York, NY, USA, 2017. Association for Computing Machinery.
- [10] Anonymous et al. Anonymous to preserve double blind review, 2020.
- [11] David Tse and Pramod Viswanath. *Fundamentals of wireless communication*. Cambridge university press, 2005.
- [12] Zhihong Luo, Qiping Zhang, Yunfei Ma, Manish Singh, and Fadel Adib. 3d backscatter localization for fine-grained robotics. In *16th {USENIX} Symposium on Networked Systems Design and Implementation ({NSDI} 19)*, pages 765–782, 2019.
- [13] Colleen Josephson, Bradley Barnhart, Sachin Katti, Keith Winstein, and Ranveer Chandra. Rf soil moisture sensing via radar backscatter tags. *arXiv preprint arXiv:1912.12382*, 2019.
- [14] Arduino Due. <https://store.arduino.cc/due>. Accessed: 2020-09-01.
- [15] a National Instruments Company Ettus Research. USRP: Universal software defined radio peripheral networked series. <https://www.ettus.com/product-categories/usrp-networked-series/>. Accessed: 2020-09-01.
- [16] Swadhin Pradhan, Eugene Chai, Karthikeyan Sundaresan, Lili Qiu, Mohammad A Khojastepour, and Sampath Rangarajan. Rio: A pervasive rfid-based touch gesture interface. In *Proceedings of the 23rd Annual International Conference on Mobile Computing and Networking*, pages 261–274, 2017.
- [17] Chuhan Gao, Yilong Li, and Xinyu Zhang. Livetag: Sensing human-object interaction through passive chipless wifi tags. In *15th {USENIX} Symposium on Networked Systems Design and Implementation ({NSDI} 18)*, pages 533–546, 2018.
- [18] Sandeep KS Gupta, Suresh Lalwani, Yashwanth Prakash, E Elsharawy, and Loren Schwiebert. Towards a propagation model for wireless biomedical applications. In *IEEE International Conference on Communications, 2003. ICC'03.*, volume 3, pages 1993–1997. IEEE, 2003.
- [19] Ilka Dove. Analysis of radio propagation inside the human body for in-body localization purposes. Master’s thesis, University of Twente, 2014.

- [20] Deepak Vasisht, Guo Zhang, Omid Abari, Hsiao-Ming Lu, Jacob Flanz, and Dina Katabi. In-body backscatter communication and localization. In *Proceedings of the 2018 Conference of the ACM Special Interest Group on Data Communication*, pages 132–146, 2018.
- [21] A. Sani, M. Rajab, R. Foster, and Y. Hao. Antennas and propagation of implanted rfids for pervasive healthcare applications. *Proceedings of the IEEE*, 98(9):1648–1655, 2010.
- [22] Nazim Haouchine, Winnie Kuang, Stephane Cotin, and Michael Yip. Vision-based force feedback estimation for robot-assisted surgery using instrument-constrained biomechanical three-dimensional maps. *IEEE Robotics and Automation Letters*, 3(3):2160–2165, 2018.
- [23] Angelica I Aviles, Samar Alsaleh, Pilar Sobrevilla, and Alicia Casals. Sensorless force estimation using a neuro-vision-based approach for robotic-assisted surgery. In *2015 7th International IEEE/EMBS Conference on Neural Engineering (NER)*, pages 86–89. IEEE, 2015.
- [24] Javad Dargahi, Saeed Sokhanvar, Siamak Najarian, and Siamak Arbatani. *Tactile Sensing and Displays: Haptic Feedback for Minimally Invasive Surgery and Robotics*. John Wiley & Sons, 2012.
- [25] Allison M Okamura. Haptic feedback in robot-assisted minimally invasive surgery. *Current opinion in urology*, 19(1):102, 2009.
- [26] Carol E Reiley, Takintope Akinbiyi, Darius Burschka, David C Chang, Allison M Okamura, and David D Yuh. Effects of visual force feedback on robot-assisted surgical task performance. *The Journal of thoracic and cardiovascular surgery*, 135(1):196–202, 2008.
- [27] Shanu N Kothari, Brian J Kaplan, Eric J DeMaria, Timothy J Broderick, and Ronald C Merrell. Training in laparoscopic suturing skills using a new computer-based virtual reality simulator (mist-vr) provides results comparable to those with an established pelvic trainer system. *Journal of laparoendoscopic & advanced surgical techniques*, 12(3):167–173, 2002.
- [28] M Zhou, S Tse, A Derevianko, DB Jones, SD Schwaitzberg, and CGL Cao. Effect of haptic feedback in laparoscopic surgery skill acquisition. *Surgical endoscopy*, 26(4):1128–1134, 2012.
- [29] Michael Yip and David Camarillo. Model-less hybrid position/force control: a minimalist approach for continuum manipulators in unknown, constrained environments. *IEEE Robotics and Automation Letters*, 2016.
- [30] Gregory Tholey, Jaydev P Desai, and Andres E Castellanos. Force feedback plays a significant role in minimally invasive surgery: results and analysis. *Annals of surgery*, 241(1):102, 2005.
- [31] Ravinder S Dahiya and Maurizio Valle. *Robotic tactile sensing: technologies and system*. Springer Science & Business Media, 2012.
- [32] Homa Alemzadeh, Jaishankar Raman, Nancy Leverson, Zbigniew Kalbarczyk, and Ravishankar K Iyer. Adverse events in robotic surgery: a retrospective study of 14 years of fda data. *PloS one*, 11(4):e0151470, 2016.
- [33] Anibal Francone, Jason Mingyi Huang, Ji Ma, Tsu-Chin Tsao, Jacob Rosen, and Jean-Pierre Hubschman. The effect of haptic feedback on efficiency and safety during preretinal membrane peeling simulation. *Translational vision science & technology*, 8(4):2–2, 2019.
- [34] Ilana Nisky, Felix Huang, Amit Milstein, Carla M Pugh, Ferdinando A Mussa-Ivaldi, and Amir Karniel. Perception of stiffness in laparoscopy—the fulcrum effect. *Studies in health technology and informatics*, 173:313, 2012.
- [35] Aude Billard and Danica Kragic. Trends and challenges in robot manipulation. *Science*, 364(6446), 2019.
- [36] Zhen Deng, Yannick Jonetzko, Liwei Zhang, and Jianwei Zhang. Grasping force control of multi-fingered robotic hands through tactile sensing for object stabilization. *Sensors*, 20(4):1050, 2020.
- [37] Wenzhen Yuan, Siyuan Dong, and Edward H Adelson. Gelsight: High-resolution robot tactile sensors for estimating geometry and force. *Sensors*, 17(12):2762, 2017.
- [38] Yu She, Sandra Q Liu, Peiyu Yu, and Edward Adelson. Exoskeleton-covered soft finger with vision-based proprioception and tactile sensing. In *2020 IEEE International Conference on Robotics and Automation (ICRA)*, pages 10075–10081. IEEE, 2020.
- [39] Wei Chen, Heba Khamis, Ingvars Birznieks, Nathan F Lepora, and Stephen J Redmond. Tactile sensors for friction estimation and incipient slip detection—toward dexterous robotic manipulation: A review. *IEEE Sensors Journal*, 18(22):9049–9064, 2018.

- [40] Hiroshi Ishii. The tangible user interface and its evolution. *Communications of the ACM*, 51(6):32–36, 2008.
- [41] Yang Zhang, Yasha Iravantchi, Haojian Jin, Swarun Kumar, and Chris Harrison. Sozu: Self-powered radio tags for building-scale activity sensing. In *Proceedings of the 32nd Annual ACM Symposium on User Interface Software and Technology*, pages 973–985, 2019.
- [42] Chuhan Gao, Yilong Li, and Xinyu Zhang. Livetag: Sensing human-object interaction through passive chipless wi-fi tags. *GetMobile: Mobile Computing and Communications*, 22(3):32–35, 2019.
- [43] Cheng Chi, Xuguang Sun, Ning Xue, Tong Li, and Chang Liu. Recent progress in technologies for tactile sensors. *Sensors*, 18(4):948, 2018.
- [44] Ryosuke Matsuzaki and Akira Todoroki. Wireless flexible capacitive sensor based on ultra-flexible epoxy resin for strain measurement of automobile tires. *Sensors and Actuators A: Physical*, 140(1):32–42, 2007.
- [45] T Hoffmann, B Eilebrecht, and S Leonhardt. Respiratory monitoring system on the basis of capacitive textile force sensors. *IEEE sensors journal*, 11(5):1112–1119, 2010.
- [46] Chen Li, Qiulin Tan, Pinggang Jia, Wendong Zhang, Jun Liu, Chenyang Xue, and Jijun Xiong. Review of research status and development trends of wireless passive lc resonant sensors for harsh environments. *Sensors*, 15(6):13097–13109, 2015.
- [47] Qing-An Huang, Lei Dong, and Li-Feng Wang. Lc passive wireless sensors toward a wireless sensing platform: status, prospects, and challenges. *Journal of Microelectromechanical Systems*, 25(5):822–841, 2016.
- [48] Clementine M Boutry, Levent Beker, Yukitoshi Kaizawa, Christopher Vassos, Helen Tran, Allison C Hinckley, Raphael Pfattner, Simiao Niu, Junheng Li, Jean Claverie, et al. Biodegradable and flexible arterial-pulse sensor for the wireless monitoring of blood flow. *Nature biomedical engineering*, 3(1):47–57, 2019.
- [49] Baoqing Nie, Ting Yao, Yiqiu Zhang, Jian Liu, and Xinjian Chen. A droplet-based passive force sensor for remote tactile sensing applications. *Applied Physics Letters*, 112(3):031904, 2018.
- [50] Marco Baù, Marco Demori, Marco Ferrari, and Vittorio Ferrari. Contactless readout of passive lc sensors with compensation circuit for distance-independent measurements. In *Multidisciplinary Digital Publishing Institute Proceedings*, volume 2, page 842, 2018.
- [51] Haining Li, Jiexiong Ding, Siqi Wei, Bowen Chu, Lichao Guan, Li Du, Guangmin Liu, and Jianguo He. A miniature layered saw contact stress sensor for operation in cramped metallic slits. *Instruments and Experimental Techniques*, 61(4):610–617, 2018.
- [52] Xiaohua Yi, Terence Wu, Yang Wang, Roberto T Leon, Manos M Tentzeris, and Gabriel Lantz. Passive wireless smart-skin sensor using rfid-based folded patch antennas. *International Journal of Smart and Nano Materials*, 2(1):22–38, 2011.
- [53] Trang T Thai, Herve Aubert, Patrick Pons, Manos M Tentzeris, and Robert Plana. Design of a highly sensitive wireless passive rf strain transducer. In *2011 IEEE MTT-S International Microwave Symposium*, pages 1–4. IEEE, 2011.
- [54] JR Humphries and DC Malocha. Passive, wireless saw ofc strain sensor. In *2012 IEEE International Frequency Control Symposium Proceedings*, pages 1–6. IEEE, 2012.
- [55] Lijun Teng, Kewen Pan, Markus P Nemitz, Rui Song, Zhirun Hu, and Adam A Stokes. Soft radio-frequency identification sensors: Wireless long-range strain sensors using radio-frequency identification. *Soft robotics*, 6(1):82–94, 2019.
- [56] Nicolai Marquardt, Alex S Taylor, Nicolas Villar, and Saul Greenberg. Rethinking rfid: awareness and control for interaction with rfid systems. In *Proceedings of the SIGCHI Conference on Human Factors in Computing Systems*, pages 2307–2316, 2010.
- [57] Alanson P Sample, Daniel J Yeager, and Joshua R Smith. A capacitive touch interface for passive rfid tags. In *2009 IEEE International Conference on RFID*, pages 103–109. IEEE, 2009.
- [58] Timothy M Simon, Bruce H Thomas, Ross T Smith, and Mark Smith. Adding input controls and sensors to rfid tags to support dynamic tangible user interfaces. In *Proceedings of the 8th International Conference on Tangible, Embedded and Embodied Interaction*, pages 165–172, 2014.
- [59] Albrecht Schmidt, H-W Gellersen, and Christian Merz. Enabling implicit human computer interaction: a wearable rfid-tag reader. In *Digest of Papers. Fourth International Symposium on Wearable Computers*, pages 193–194. IEEE, 2000.

- [60] Hanchuan Li, Eric Brockmeyer, Elizabeth J Carter, Josh Fromm, Scott E Hudson, Shwetak N Patel, and Alanson Sample. Paperid: A technique for drawing functional battery-free wireless interfaces on paper. In *Proceedings of the 2016 CHI Conference on Human Factors in Computing Systems*, pages 5885–5896, 2016.
- [61] Hanchuan Li, Can Ye, and Alanson P Sample. Id-sense: A human object interaction detection system based on passive uhf rfid. In *Proceedings of the 33rd Annual ACM Conference on Human Factors in Computing Systems*, pages 2555–2564, 2015.
- [62] Michael Steer. *Microwave and RF design*. NC State University, 2019.

9 Appendix

For an air substrate microstrip transmission line, we have the following equation which governs the impedance matching, $Z = 60 \ln \left[\frac{6h}{w} + \sqrt{1 + \left(\frac{2h}{w} \right)^2} \right]$, where h is the vertical separation between signal and ground trace, and w is the width of the signal trace [62]. Setting $Z = 50 \Omega$ in the above equation, gives us the operating $\frac{h}{w}$ ratio to be approximately 5 : 1. In order to interface SMA connectors to the air-substrate microstrip line designed, we have to increase the width of the ground trace so that the bottom legs of the SMA connector can be soldered directly to the ground trace.

However, we notice some deviation from this ratio when the width of ground trace is increased to allow for easier interfacing with SMA connectors. We simulate the sensor in Ansys HFSS (Fig. 19) to determine this deviation, and observe that the ideal operating ratio shifts to about 4:1 instead of 5:1 when the width of ground trace is increased.

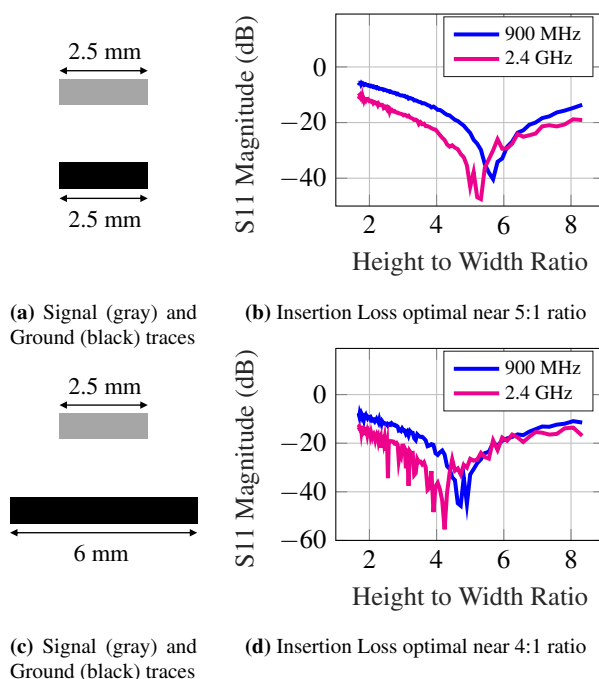


Figure 19: HFSS simulation results: as the ground layer width is increased to allow for easier interfacing with the SMA connector, the ideal height:width ratio decreases from 5:1 to 4:1.